Fine structure of the intracochlear potential field

I. The silent current

Michael Zidanic and William E. Brownell

Departments of Otolaryngology-Head and Neck Surgery, and Neuroscience, The Center for Hearing Sciences, The Johns Hopkins University, Baltimore, Maryland 21205-2195 USA

ABSTRACT Field potentials were recorded along radial tracks in scala tympani and scala vestibuli of the guinea-pig cochlea. A current density analysis revealed standing current density profiles that were qualitatively similar between animals and between the second and third cochlear turns. Radial standing current densities were greatest at or near the spiral ligament. All the scala vestibuli current density profiles were scaled versions of one another while the scala tympani current density profiles showed more variability. Acoustic stimuli modulated the standing current and there was a cochlear microphonic current density peak in scala tympani near the organ of Corti. The results are summarized with a current-density field line model, the key element of which is a constant current pumped into scala media by the stria vascularis. The standing potential gradients drive current from each perilymphatic chamber into the spiral ligament en route to the lateral surface of the stria vascularis. The strial current is divided between the receptor cell pathway and leakage pathways. The standing current through the leakage pathways is indirectly modulated by acoustic stimulation through the modulation of the endocochlear potential. The reciprocal modulation of current between hair cell and leakage pathways suggests that the stria vascularis maintains a constant current during acoustic stimulation. The cochlear standing current is similar to the retinal dark current in its importance for sensory transduction but the fact that the silent current is generated by the stria vascularis and not the receptor cells provides significant benefits for the detection of mechanical stimuli.

INTRODUCTION

Living cells expend metabolic energy to maintain large electrochemical gradients across their plasma membranes. Changes in membrane permeability to ions that are out of electrochemical equilibrium result in transmembrane ionic currents. The ionic currents are balanced by oppositely-directed capacitative currents that charge or discharge the membrane. The geometric relations among all such current sources and sinks with respect to resistive elements of the extracellular space determines the direction and density of extracellular current. The extracellular potentials associated with such currents are generally very small due to the low resistivity of extracellular fluid. However, the ionic channels that effect permeability changes can be concentrated at discrete locations in the plasma membrane (such as sodium channels at the nodes of Ranvier), resulting in large local extracellular current densities. The simultaneous activation of a permeability change in many neurons with similar spatial orientation can result in even larger field potentials generated by very high current densities.

In contrast to transient field potentials generated by neuronal currents, some tissues maintain continuous extracellular potential gradients. The dark current of the vertebrate retina is an example of a standing extracellular current with an important sensory function (Penn and Hagins, 1969; Hagins et al., 1970). The dark current is generated by sodium ions that are pumped out of the rod inner segments and that reenter the photoreceptor through sodium channels in the outer segment. The spatial separation of the current sources and sinks generates a standing intracellular current and an oppositely-directed extracellular current. This paper describes a standing current in the mammalian cochlea that we call the "silent current". Like the retinal dark current, it is large in the absence of a sensory stimulus and is modulated by an adequate stimulus. An important difference is that the dark current is generated by the photoreceptor cells themselves while the silent current is generated by an organ (the stria vascularis) situated nearly a half-millimeter away from the mechanoreceptors of the organ of Corti.

Scala tympani and scala vestibuli are perilymph-filled chambers of the mammalian inner ear (see Figs. 2 and 14). The ionic composition of perilymph resembles that of cerebral fluid, with which it is continuous. The endolymph of scala media is a most unusual extracellular fluid

Dr. Zidanic's current address is INSERM Unit 254, Laboratoire de Neurophysiologie Sensorielle, U.S.T.L. Place Eugene Bataillon, 34060 Montpellier Cedex, France.

due to its high-potassium, low-sodium ion concentrations (Smith et al., 1954; Salt and Konishi, 1986) combined with an electric potential 80 mV more positive than perilymph (von Békésy, 1952). Tasaki and Spyropoulos (1959) were the first to demonstrate that the stria vascularis was responsible for the endocochlear potential (EP). The energy required to sustain the EP is large as can be inferred by the degree to which this organ is vascularized and its high ($Na^+ + K^+$)-ATPase activity (Kuijpers and Bonting, 1969). Paracellular endolymph leakage is minimized by tight junctions between all cells that border scala media (Jahnke, 1975; Gulley and Reese, 1976; Iurato et al., 1976). Horseradish-peroxidase experiments demonstrate that there is little resistance for the movement of perilymph up to the tight junctions and that the fluid in the highly porous spiral ligament as well as in the organ of Corti communicates readily with perilymph (Duvall and Sutherland, 1972; Siegel and Brownell, 1986).

Davis (1953) was the first to suggest the presence of a standing current in the cochlea generated by the stria vascularis. He postulated the current would exit scala media through a mechanically dependent variable resistance associated with the stereocilia of the hair cells in the organ of Corti and flow radially across scala tympani, through the spiral ligament, and back to the stria vascularis, completing a local circuit (as in Fig. 14). The cochlear microphonic (CM) was then explained as the acoustically-evoked field potential resulting from the modulation of standing current in the extracellular space. Tasaki et al. (1954) tried to measure standing currents in scala tympani but were unsuccessful. No further attempts have been made despite many experiments that otherwise support Davis' model of transduction (see Brownell et al., 1986, for a review).

Several experiments provide indirect evidence in support of a standing current. When the EP is lowered after administering the loop-diuretic furosemide, the spontaneous activity of auditory nerve fibers concomitantly decreases (Sewell, 1984), consistent with an EP-dependent depolarizing standing current through inner hair cells. Additional evidence for a standing current through the inner hair cells comes from the data of Liberman and Dodds (1984), who exposed animals to loud sounds that were sufficient to cause threshold shifts. Auditory nerve fibers were characterized, labeled with horseradish-peroxidase, and traced back to the inner hair cells that they innervated. The number of stereocilia on the innervated inner hair cell were counted, and spontaneous activity was correlated with the number of stereocilia that remained, suggesting that ion flux through each stereocilium contributes a small depolarizing current to the inner hair cell.

Evidence for a standing current through the outer hair cells comes from crossed olivocochlear bundle stimulation experiments. When the crossed olivocochlear bundle efferents to the outer hair cells are stimulated with a train of shocks, the EP decreases (Fex, 1967; Teas et al., 1970). This result is consistent with a standing current through the outer hair cells in silence that is increased by an efferent-induced conductance increase of the basolateral membrane of the outer hair cell (Geisler, 1974). The finding that the CM to low-frequency stimuli increases with efferent stimulation (Fex, 1959; Teas et al., 1970) is also consistent with a significant current through the outer hair cells.

We have used a current density analysis technique similar to that used to demonstrate the existence of a dark current in the vertebrate retina (Penn and Hagins, 1969; Hagins et al., 1970) and were able to demonstrate transient click-evoked radial current densities in scala tympani of the guinea-pig cochlea (Brownell et al., 1983). Current density results are presented here that represent the first direct measurements of standing currents in the cochlea. Our results confirm portions of Davis' original hypothesis and provide new information about the fine structure of the ongoing ion movement in the cochlea and the energetics of cochlear transduction. Preliminary versions of these results have been presented in abstract form (Zidanic et al., 1984, 1985, 1987).

METHODS

Animal preparation

Healthy guinea pigs weighing 200–500 g were anesthetized with initial doses of 18 mg/kg sodium pentobarbital and 0.25 ml/kg Innovar-Vet (fentanyl, 0.1 mg/kg; droperidol 5 mg/kg). Anesthesia was maintained by administering a sustaining dose each hour, alternating between pentobarbital and Innovar at one-third the induction doses. All of the surgical procedures and electrophysiological recordings were conducted in a sound isolation chamber heated to 32–35°C to prevent hypothermia of the animal and of the exposed cochlea. The animal was secured to the recording table with a head bar, the external auditory meatus was dissected free, and the cochlea was exposed by a ventral approach. The tensor tympani and stapedius muscles were severed. The animal was then paralyzed with Flaxedial (gallamine triethiodide, 5 mg/kg) and artificially respired.

The physiological state of the cochlea was monitored by measuring tone-evoked compound action potential (CAP) thresholds from a copper wire placed on the bone near the round window. Sound pressure in the external auditory meatus was measured through a calibrated probe tube microphone. Fig. 1 (*top*) shows the results of this initial CAP determination in a sample of 28 guinea pigs. The average threshold in the frequency range 500–5,000 Hz was 40–45 dB SPL (sound pressure level *re* 20 μPa), although the most sensitive animals could have thresholds in the 30–35 dB SPL range. The guinea-pig CAP thresholds reported here are within the range that have been measured by other investigators (Johnstone et al., 1979; Robertson et al., 1980). The most sensitive auditory neurons for a particular characteristic frequency (CF) have thresholds 20 dB lower than the CAP threshold determined for the same frequency (Johnstone et al., 1979).

A fenestra of 40–100 μm in diameter was then made in the otic capsule to gain access to scala tympani or scala vestibuli of the second or third turn. The fenestra was made by alternately hand-drilling with a four-sided awl and a fine-tipped pick. Bone chips were cleared with a fine cotton wick as the hole was drilled deeper. The exposure was enlarged until an opening to the spiral ligament was visualized. Threshold shifts after this procedure are shown in Fig. 1 (*bottom*) for a population of 19 guinea pigs. Third-turn exposures (15 ± 0.5 mm from the base; CF, 0.8–1.0 kHz) could generally be made without losing more than 5 dB, whereas second-turn exposures (11.5 ± 0.5 mm from the base) usually resulted in threshold shifts of 5–10 dB at frequencies near CF (2.5–4.5 kHz).

Electric recording

Micropipettes were fabricated to have shanks of 500–800 μm that were 1–2 μm at the tip, and widened to no more than 30 μm along the length of the shank. Tip potentials and ion diffusion were minimized by filling the pipettes with a solution that ionically resembles perilymph (155 mM NaCl, 4 mM KCl). Micropipette holders were filled with electrolyte at least 1 h before recording to allow the junction potential of the Ag/AgCl electrodes to stabilize. Potentials were amplified (×1,000) and digitized with a 12-bit A/D converter (±10 V dynamic range).

Pipettes were advanced and withdrawn with a piezoelectric microdrive system. The desired orientation of the pipette was always along a radial path from the lateral wall towards the modiolar axis of the cochlea. The angle of the track with respect to the modiolar axis depended on the cochlear chamber to be studied. In scala-tympani experiments, the optimal orientation was along a path parallel to the basilar membrane, whereas in scala-vestibuli experiments, the apex of the cochlea was tilted up ~30° to achieve a track parallel to Reissner's membrane. These orientations define the radial component of a local Cartesian coordinate system in scala tympani and in scala vestibuli (labeled i_r in Fig. 2). The vertical component, i_v, is oriented orthogonally to the radial component and points towards the apex of the cochlea.

In 12 experiments the cochlea was removed from the animal after the experiment was terminated. The specimen was then fixed, dehydrated, embedded in celloidin, and sectioned approximately parallel to the electrode track. The example shown in Fig. 2 is traced from the only case where the electrode track through the spiral ligament was recovered. In this third-turn scala-tympani experiment the electrode track was at an angle of ~30° from the basilar membrane. Because this type of reconstruction could not be done for all experiments, the data from different experiments were not corrected for any deviations from the defined radial direction (i.e., parallel to the basilar membrane or parallel to Reissner's membrane).

Also illustrated in Fig. 2 is a fixed pipette (labeled the spiral-ligament

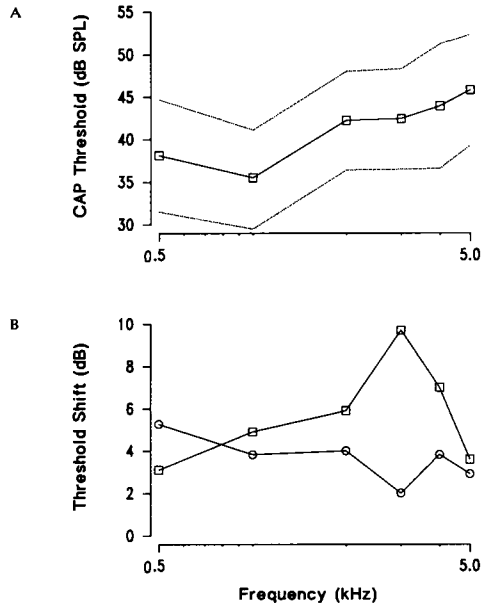

FIGURE 1 Initial CAP thresholds and threshold shifts after otic capsule surgery. (*A*) CAP threshold for frequency range 0.5–5.0 kHz averaged over 28 guinea pigs. Round-window potentials were averaged in response to 25–50 repetitions of 20-ms tone bursts with a rise time of 1 ms. The tone stimulus was presented at a random phase relative to the initiation of A/D conversion to filter out the CM. Threshold was defined as the sound pressure level *re* 20 μPa (dB SPL) required to elicit a CAP with a 5-μV peak amplitude. Dotted lines indicate one standard deviation from the mean. (*B*) CAP threshold shifts after making a 40–100-μm fenestra in the otic capsule. (*Squares*) Average of nine second-turn exposures. (*Circles*) Average of 11 third-turn exposures.

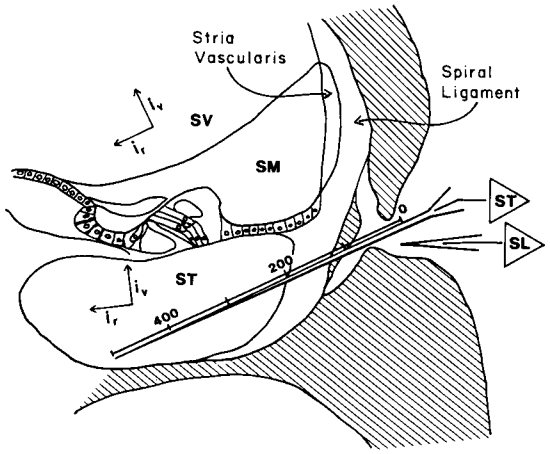

FIGURE 2 Camera lucida drawing of a celloidin-embedded section through the third-turn exposure of an experimental animal (GP82). Scala vestibuli (*SV*), scala media (*SM*), and scala tympani (*ST*) are labeled. Reissner's membrane separates SV from SM. The movable pipette is shown at the modiolar end of a reconstructed electrode track (*ST*). Because the tissue was sectioned obliquely relative to the radial path of the electrode track, the pipette crossed this plane of section only at the fenestra over the spiral ligament. The orientation of the pipette relative to the basilar membrane was determined by the appearance of a hole in the spiral ligament on sections that were 40–60 μm closer to the mid-modiolar plane. The large bone chip that sheared off from the otic capsule extended ~20 μm on both side of the section shown. The spiral-ligament pipette that monitored potentials in the fluid that collects over the otic capsule fenestra is also shown. The scale above the *ST* pipette is in microns. The vectors representing the two-dimensional local coordinate system are shown deep in ST and in SV. The radial dimension is parallel to the basilar membrane in ST. The coordinate system in SV is tilted relative to the ST system so that the radial dimension is parallel to Reissner's membrane. The third dimension of the coordinate system, the longitudinal component, projects orthogonal to the plane of the page.

[SL] electrode) which was placed in the drop of fluid that formed over the otic-capsule fenestration. The formation of the drop results from hydrostatic pressure within the cochlea that forces perilymph out of the exposure. Eventually, cerebrospinal fluid replaces the leaking perilymph. The spiral-ligament pipette was broken back several hundred microns to a tip size of ~10 μm to achieve a lower impedance and noise level. The fixed electrode served both as a local DC reference and also as a monitor of the CM.

The depth of the fluid layer from the air-perilymph interface to the surface of the spiral ligament could vary between 100 and 200 μm, depending on the shape and location of the exposure. The movable pipette was advanced ~40 μm from the surface before beginning the 500–700-μm recording track to help ensure that the pipette would remain in the fluid upon withdrawal to the starting point. This starting point is assigned a value of zero, and all depths modiolar to this point are assigned positive values. Because it was noted in early experiments that the pipette could bend while penetrating the spiral ligament, the protocol for the later experiments was to manually advance the electrode, and then to collect data as the electrode was withdrawn in 20-μm steps under computer control. Occasionally, during withdrawal, the pipette lost electrical contact with the preparation 100–200 μm before reaching the starting point of the track. Loss of contact usually meant that the pipette had broken (some pipette fragments have appeared in histological material). Recording was aborted and the electrode repositioned when large positive DC shifts (5–70 mV) or large negative DC shifts (30–80 mV) were encountered over a limited distance on some scala-tympani tracks that probably came close to or penetrated scala media. The negative DC shifts were very unstable and were most likely intracellular potentials associated with hair cells or supporting cells in the organ of Corti.

Data analysis: DC potential profiles

At each 20-μm step along the electrode track one or more acoustic stimuli were presented to the animal. The evoked responses picked up by the fixed and movable electrodes were simultaneously averaged (10–25 repetitions). The acoustic stimulus was delayed by 2 ms relative to the initiation of A/D conversion in order to record both the baseline DC potential and evoked response. The A/D values were averaged over this 2-ms interval to compute a DC baseline for each electrode and stimulus combination. If more than one acoustic stimulus was presented, then the DC potential for each electrode was computed by averaging the DC baselines preceding the evoked responses. In the equations that follow, the averaged DC value on the movable electrode at depth x_i is symbolized $DC_{mv}(x_i)$ and the averaged DC value on the fixed electrode when the movable electrode was at depth x_i is symbolized $DC_{fx}(x_i)$.

The major source of DC potential fluctuation was drift in the ground electrode junction potential. The effect of this drift was minimized by referencing the DC potential recorded by the movable electrode to the DC potential recorded by the fixed electrode as follows:

$$DC_{mv\text{-}fx}(x_i) = DC_{mv}(x_i) - DC_{fx}(x_i), \quad (1)$$

where $x_i = 0$ μm, $x_2 = 20$ μm, . . . , $x_d = 20\,(d\text{-}1)$ μm. The results of this operation are illustrated in Fig. 3. Multiple DC profiles are plotted from sequential excursions along the same track. The profiles show less scatter when the fixed electrode is used as the DC reference (*bottom*) instead of the ground electrode (*top*).

In addition to drift in the junction potential of the ground electrode, there was also long-term DC drift of the potential between the fixed and movable electrodes. It was necessary to minimize this drift by subtracting the DC potential difference between the two electrodes when the movable electrode was at the starting point of the track (i.e., when the two electrodes were closest to each other) from the DC potential differences recorded along the rest of the track as follows:

$$\phi^{dc}(x_i) = DC_{mv\text{-}fx}(x_i) - DC_{mv\text{-}fx}(x_1), \quad (2)$$

for $i = 1,2, \ldots, d$. This operation effectively defines a DC reference point at the end of each withdrawal track within 40 μm of the air-perilymph interface. The DC potential is assigned a value of zero at this location and all DC potentials modiolar to this location are shifted by an amount equal to the deviation of this first point from zero. Unlike the DC-referencing operation performed in Eq. 1, this operation has no effect on the DC potential gradient calculations.

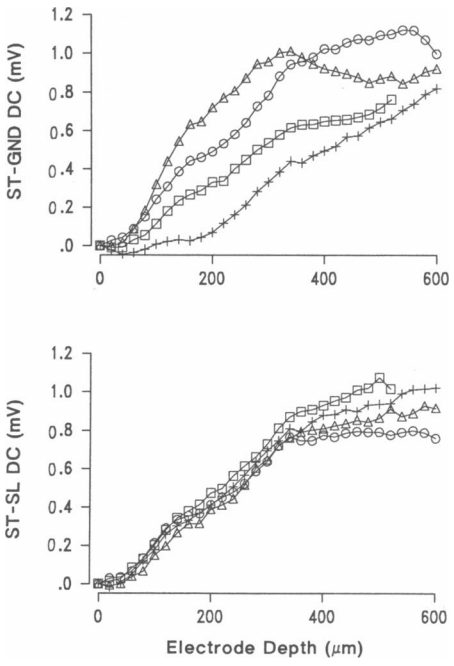

FIGURE 3 Effect of using the fixed electrode outside the spiral ligament as a local DC reference. Data from four electrode excursions along the same track in scala tympani of the second turn (GP89). DC profiles using the ground electrode as the DC reference (*top*). DC profiles using the fixed electrode as the DC reference (*bottom*).

Data analysis: DC potential gradient profiles

In a three-dimensional Cartesian coordinate system, the DC electric field $\mathbf{E}^{dc}$ at a point $\mathbf{x}$ is related to the DC potential field ϕ^{dc} by

$$\mathbf{E}^{dc}(\mathbf{x}) = -\nabla\phi^{dc}(\mathbf{x}) = -\frac{\partial\phi^{dc}(\mathbf{x})}{\partial r}\mathbf{i}_r - \frac{\partial\phi^{dc}(\mathbf{x})}{\partial v}\mathbf{i}_v - \frac{\partial\phi^{dc}(\mathbf{x})}{\partial l}\mathbf{i}_l$$

$$= E_r^{dc}(\mathbf{x})\mathbf{i}_r + E_v^{dc}(\mathbf{x})\mathbf{i}_v + E_l^{dc}(\mathbf{x})\mathbf{i}_l, \quad (3)$$

where E_r^{dc}, E_v^{dc}, and E_l^{dc} are the magnitudes of the DC electric field and $\mathbf{i}_r$, $\mathbf{i}_v$, and $\mathbf{i}_l$ are the unit vectors in the radial, vertical, and longitudinal axes, respectively. The three partial derivatives, $\partial\phi^{dc}(\mathbf{x})/\partial r$, $\partial\phi^{dc}(\mathbf{x})/\partial v$, and $\partial\phi^{dc}(\mathbf{x})/\partial l$, form the radial, vertical, and longitudinal components, respectively, of the potential gradient vector $\nabla\phi^{dc}(\mathbf{x})$ and represent the rate of change of potential with respect to space along each of the three principal axes. When these three components are vectorially combined,

a potential gradient vector $\nabla\phi^{dc}(\mathbf{x})$ is constructed that points in the direction that the potential field is maximally increasing.

Before computing the first spatial derivative, the DC potentials are digitally filtered using the following weighting function:

$$\phi_s^{dc}(x_i) = \frac{2\phi^{dc}(x_{i+1}) + 3\phi^{dc}(x_i) + 2\phi^{dc}(x_{i-1})}{7} \quad (4)$$

for $i = 2, \ldots, d\text{-}1$. The DC potentials plotted in the figures in the Results section are not smoothed. The radial component of the DC electric field E_r^{dc} is then computed from the smoothed potentials as a finite difference:

$$E_r^{dc}(x_i) = \frac{\phi_s^{dc}(x_{i-1}) - \phi_s^{dc}(x_{i+1})}{x_{i+1} - x_{i-1}}. \quad (5)$$

for $i = 3, \ldots, d\text{-}2$. This combined smoothing and finite difference algorithm has previously been referred to as D3 smoothing (Brownell et al., 1983) of the first spatial derivative following the nomenclature introduced for smoothing formulas of the second spatial derivative (Freeman and Nicholson, 1975).

Because the origin of the local coordinate system in the cochlea is taken to be the air-perilymph interface at the site of the otic-capsule fenestra and the positive radial direction is toward the modiolus, it follows that the radial unit vector of the electric field is oriented towards the modiolus. Thus, a positive electric field is a driving force for current towards the modiolus, and a negative electric field drives current toward the spiral ligament. The terms "potential gradient" and "current" are used interchangably with electric field when describing and discussing the results of this study.

The radial component of the DC current density field at a point $\mathbf{x}$, $J_r^{dc}(\mathbf{x})$, is related to the DC electric field by Ohm's law,

$$J_r^{dc}(\mathbf{x}) = g_r^{dc}(\mathbf{x}) E_r^{dc}(\mathbf{x}), \quad (6)$$

where $g_r^{dc}(\mathbf{x})$ is the resistive component of the conductivity tensor in the radial direction at the point $\mathbf{x}$. If there is a conductivity gradient along the radial track, i.e., $\partial g_r^{dc}(\mathbf{x})/\partial r \neq 0$, then the shape of the radial current density profile will be different from the shape of the radial DC electric field profile. Although conductivity gradients are not expected within the fluid spaces of the cochlea, it is likely that the conductivity of the spiral ligament tissue is less than that of perilymph.

Translation and averaging of DC gradient profiles

To compare DC gradient profiles across experiments, we averaged profiles to reduce the data collected during an experiment to a single representative profile. To compensate for absolute changes in the position of the electrode with respect to the cochlea that occured over the course of the experiment, some DC profiles were translated along the radial axis (i.e., the abcissa) before averaging. This translation procedure is illustrated in Fig. 4. Four DC potential profiles that were collected over a 3-h period in a second-turn scala-tympani experiment are shown in *A* (uncorrected depth). Potential gradients were calculated from the profiles of *A* and are shown below in *C*. The peak of the DC gradient varies from depth 60 (*circles*) to depth 140 (*triangles*). The average of these DC gradients would result in a peak wider than any of the individual profiles. However, when the data are first translated by a multiple of 20 μm to make the DC gradient peaks coincide (*B* and *D*), the profiles are reproducible in the region of the peak. Standard deviations were calculated for these two sets of data, translated versus untranslated. In the region of the peak (0–200 μm), the average of the translated DC gradients has a standard deviation of <1 V/m compared

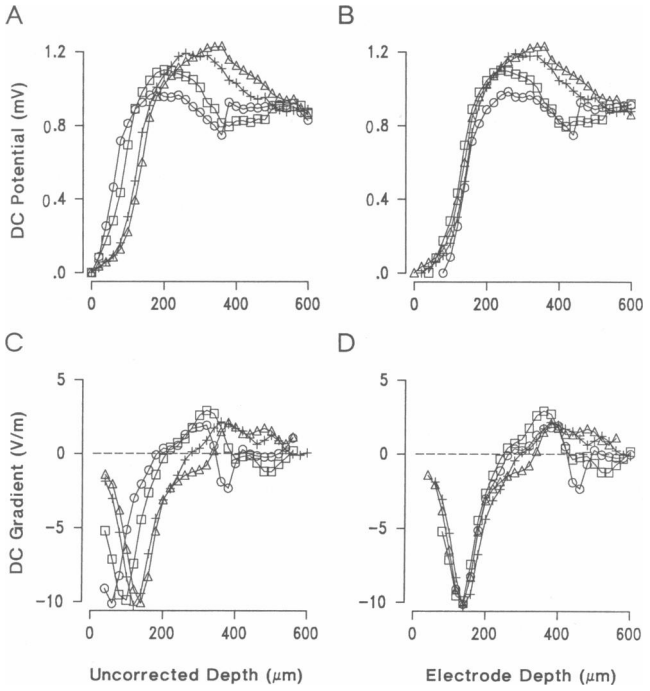

FIGURE 4 Translation operation that compensated for electrode-positioning errors that may have occured during the course of some experiments. Data from four electrode excursions along the same track in scala tympani of the second turn over a 3-h period (GPA9). Data on right were translated by a multiple of 20 μm that made the DC gradient peaks coincide. Translation factors were as follows (in micrometers): (□) +40; (○) +80; (△) 0; (+) +20. (*A*) Untranslated DC profiles. (*B*) Translated DC profiles. (*C*) Untranslated DC gradient profiles. (*D*) Translated DC gradient profiles.

to 2–3 V/m for the untranslated data. Outside the peak region in the 200–600-μm range, the standard deviation is ~1 V/m for both sets of data, indicating that the translation operation makes the average no worse in this region.

With a recording time of 1–3 h, it was possible to perform 5–15 complete excursions along the same electrode track. While all of the DC profiles recorded in a given experiment had the same general shape, there were usually a few profiles that either had unusual DC shifts or a much larger or smaller DC shift than the majority of the other profiles. Two examples of unusual DC shifts are shown: (*a*) In Fig. 4 (*top right*) the GPA9 profile represented by circles in the 440–460-μm depth range and (*b*) in Fig. 5 (*top right*) the profile represented by squares in the GPB2 experiment in the 200–280-μm depth range. Profiles that had abrupt DC shifts >200 μV were not included in the DC gradient analysis. Two to six of the remaining profiles that fell within a median range after the translation operation were then chosen for display and averaging.

RESULTS

Scala tympani DC profiles

The scala-tympani DC profiles presented in this study are based on the analysis of DC potentials collected along 140

radial electrode excursions in 16 guinea-pig cochleas. In 14 of these cochleas a single hole was made in the otic capsule in either the second or third turn. In the two other experiments (GP83 and GP85) a hole was made over scala tympani of both the second and third turns. Two second-turn experiments and two third-turn experiments are shown in Fig. 5. Each graph of this figure shows several profiles recorded along the same track. Experiment GP94 represents the most common type of profile in the second turn. In this experiment the DC potential began to increase within 100 μm of the air-perilymph interface and then continued to rise over a 200–300-μm distance to a value of >1 mV. In the second turn this DC plateau value ranged from 1.0 to 1.6 mV (mean 1.33 ± 0.2 mV, n = 9). Experiment GPB2 was unusual because the DC continued to increase over the 600-μm length of the track. Only one other scala-tympani experiment (GP89, Fig. 3) showed a similar monotonic increase. Experiment GPA9 (Fig. 4) was the only experiment in scala tympani of the second turn where the DC potential decreased in the 300–500-μm depth range. Radial DC profiles recorded in scala tympani of the third turn were similar to those obtained in the second turn, although there was much more variation in the plateau DC value ranging between 0.2 and 2.4 mV (mean 1.43 ± 0.7 mV, n = 8). In the remaining third-turn scala-tympani experiment that was not included in these calculations, the DC potential shifted negatively by 1 mV as the electrode was advanced into scala tympani.

Scala tympani DC gradient profiles

For each experiment DC profiles were averaged and the radial gradient of the mean DC profile plotted in either Fig. 6 (second-turn data) or Fig. 7 (third-turn data). The DC gradient profiles were grouped together for plotting on the basis of the magnitude of the DC gradient peak. In all experiments shown, the DC gradient had a major negative peak (indicating that current is directed away from the modiolus) ~100–200 μm from the air-perilymph interface. The magnitude of the peak varied from 3.5 to 12 V/m in the second turn and from 1 to 18 V/m in the third turn and usually fell to near zero 300–400 μm into the track. Three exceptions were the long sloping DC profiles observed in experiments GP89, GPB2 (Fig. 6), and GP32 (Fig. 7) that resulted in very broad DC gradients that remained negative over a 500-μm distance. In six of the second-turn experiments a distinct subpeak of magnitude 1.5–4.0 V/m was present 100–200 μm modiolar to the major peak (e.g., Fig. 6, experiment

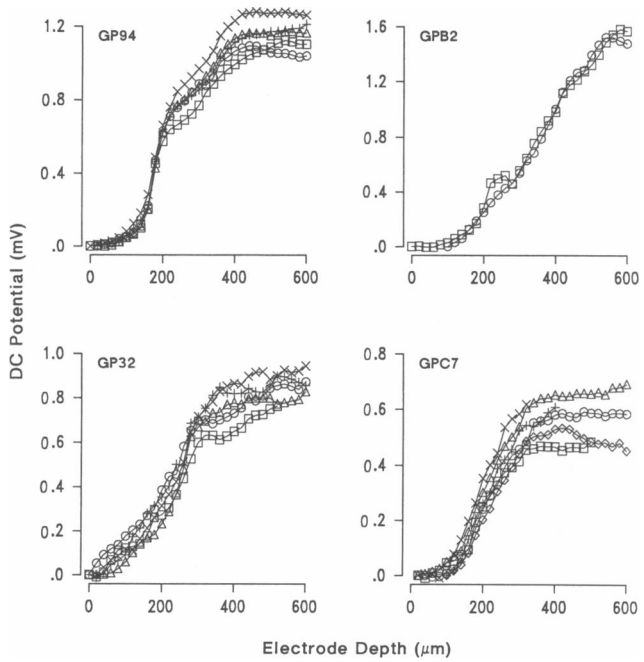

FIGURE 5 Radial DC profiles from four different experiments in scala tympani of either the second (GP94, GPB2) or third turn (GP32, GPC7). For each experiment, the DC profiles that were subjected to the DC gradient analysis are shown after they were translated according to the procedure illustrated in Fig. 4.

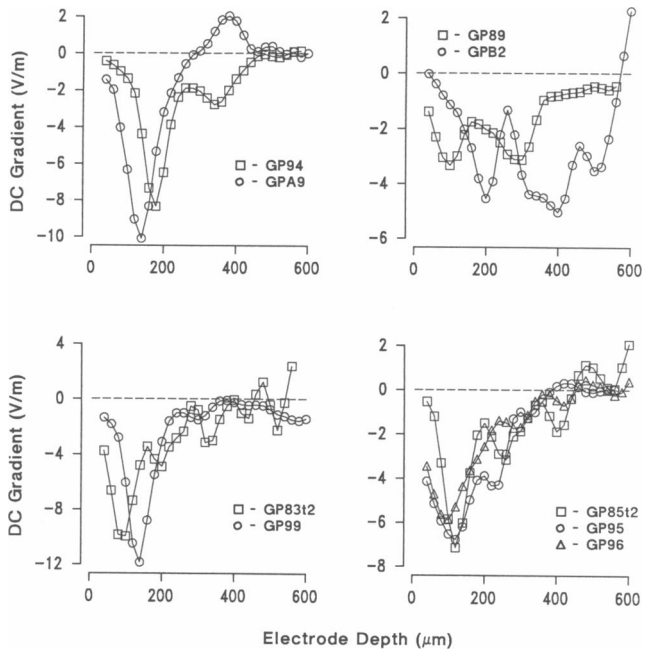

FIGURE 6 Radial DC gradient profiles fom nine experiments in scala tympani of the second turn. Each trace represents the average of two to six DC gradient profiles collected along the same track in a given animal. The profiles have been grouped together based on the magnitude and shape of the negative DC gradient peak.

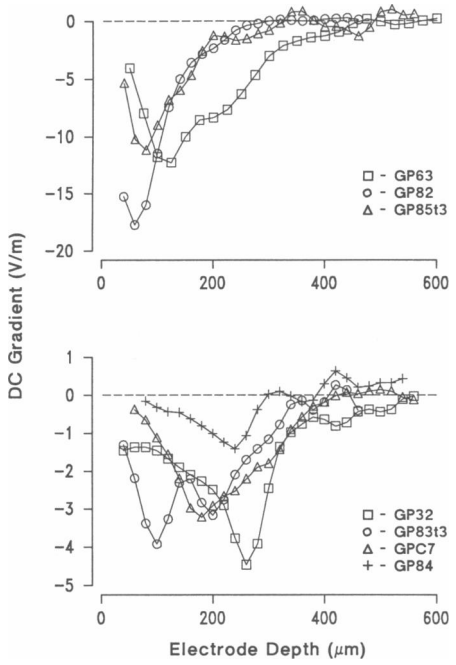

FIGURE 7 Radial DC gradient profiles from seven different experiments in scala tympani of the third turn. Three experiments with DC gradient peaks in the 10–18 V/m range (*top*). Four experiments with DC gradient peaks in the 1–5 V/m range (*bottom*).

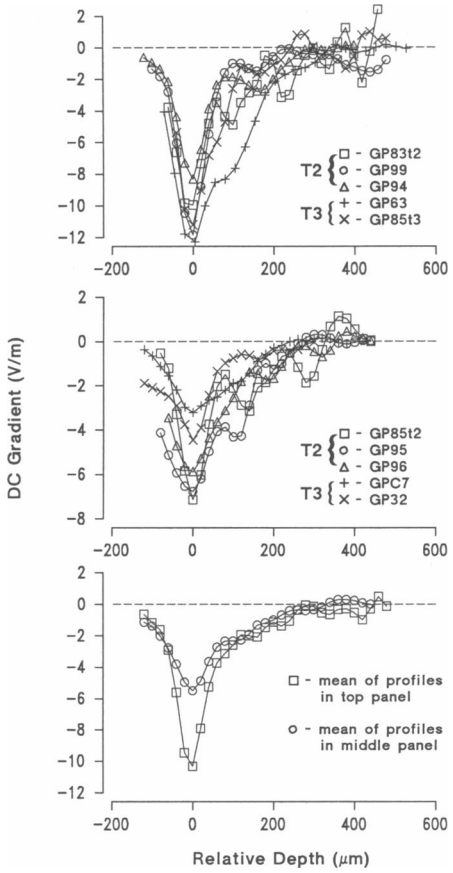

FIGURE 8 Radial DC gradient profile summary for scala tympani. Each profile has been shifted along the abscissa so that the peak of the DC gradient is plotted at depth 0 μm. (*Top*) Five profiles with DC gradient peaks in the 8–12 V/m range, three from the second turn (T2), and two from the third turn (T3). (*Middle*) Five profiles with DC gradient peaks in the 3–8 V/m range, three from the second turn (T2), and two from the third turn (T3). (*Bottom*) Four of the five profiles displayed in the top plot were averaged and are plotted as squares (GP63 was not averaged in because depth increments of 25 μm were used in that experiment). All five profiles displayed in the middle plot were averaged and are plotted as circles.

GP94, depth 340 μm). In contrast to DC gradient profiles of the second turn, only one third-turn profile had a distinct subpeak on the modiolar side of the major peak (Fig. 7, experiment GP83, depth 200 μm). Instead, the third-turn profiles tended to have a broader major peak.

In the scala-tympani experiment (GPA9, Fig. 4) where the DC potential decreased in the 300–500 μm depth range, the DC gradient profile (Fig. 6, *upper left*) went from negative to positive 300 μm into the track. This implies that current is directed toward the modiolus at locations modiolar to the zero crossing and that current is directed away from the modiolus on the spiral-ligament side of the zero crossing. One interpretation of this pattern of radial current is that a standing current source was located near the zero-crossing location in this experiment, either paracellular or transcellular current from cells situated on top of the basilar membrane, possibly in the organ of Corti.

The radial DC gradient data from scala tympani of the second and third turn are summarized in Fig. 8. All of the DC gradient profiles shown in Figs. 7 and 8 were separated into two groups based on the magnitude of the negative peak (criterion level, 8 V/m). The three DC gradient profiles that had two equal magnitude peaks (GP89, GPB2, and GP83t3) were not included, nor were the profiles that had the largest (GP82) and smallest (GP84) negative peak, nor was the single profile (GPA9) whose DC gradient changed direction. Before plotting these DC gradient profiles on the same graph, the profiles were shifted along the horizontal axis to make the negative DC gradient peaks coincide at depth 0 μm. Top panel shows five profiles in the 8–12 V/m range; middle panel shows five profiles in the 3–8 V/m range. The profiles shown in the top and middle panels were averaged and the means plotted in the bottom panel. Even though the major peaks differ by a factor of two, the modiolar slopes of the large and small types of profiles are not significantly different, implying that these two types of profiles are not simply scaled versions of one another.

Scala vestibuli DC profiles

Radial DC profiles in scala vestibuli were obtained along 85 electrode excursions in eight guinea-pig cochleas: five from the second turn and three from the third turn. Two second-turn experiments and two third-turn experiments are shown in Fig. 9. The DC profiles in scala vestibuli look quite similar to profiles in scala tympani. The DC potential increased along a shallow slope near the air-perilymph interface and then rapidly increased 1–3 mV over a 100–200-μm distance. However, the DC potential in scala vestibuli did not reach a plateau value as it usually did in scala tympani. In all experiments (except GPC8-1) the DC potential continued to increase along a shallow positive slope for the 500–600-μm length of the track

Scala vestibuli DC gradient profiles

Average radial DC potential gradients were calculated for all of the scala-vestibuli experiments and are plotted in Fig. 10 (*top*, second-turn data; *bottom*, third-turn data). In all experiments the DC gradient had a single negative peak (implying that current is directed away from the modiolus) located 100–240 μm from the air-perilymph

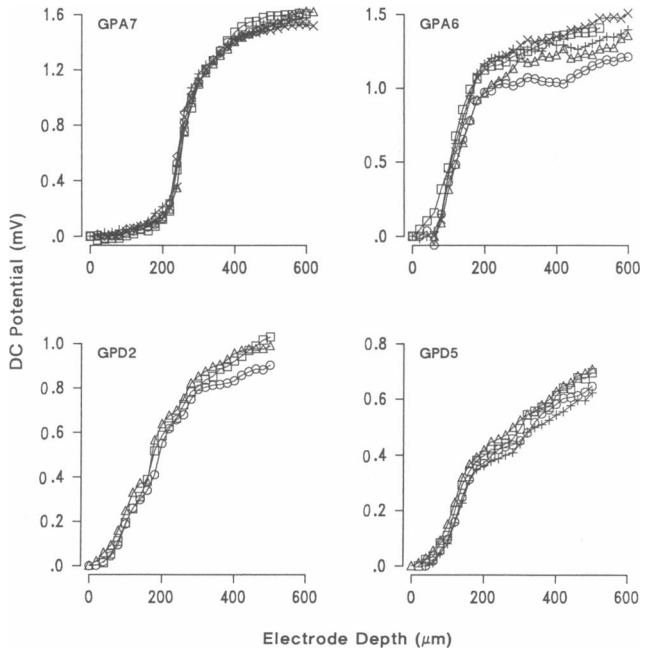

FIGURE 9 DC profiles from four different experiments in scala vestibuli of either the second (GPA6, GPA7) or third turn (GPD2, GPD5). For each experiment, the DC profiles that were subjected to the DC gradient analysis are shown after they were translated according to the procedure illustrated in Fig. 4.

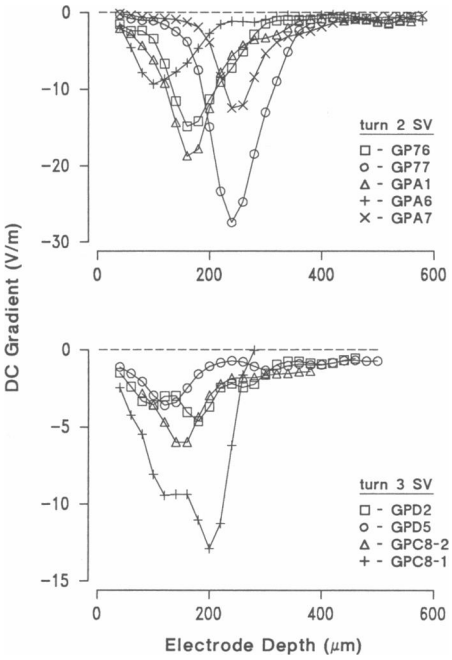

FIGURE 10 Radial DC gradient profiles from scala vestibuli. (*Top*) Second turn data. (*Bottom*) Third turn data. Data were collected along two separate tracks in experiment GPC8. A +65 mV EP was encountered at depth 500 μm of the first track (GPC8-1). The exposure was opened up toward the apical end of the cochlea and another electrode track (GPC8-2) was attempted. A +52 mV EP was encountered at depth 600 μm of the second electrode track.

interface. The magnitude of the peak varied from 10–30 V/m in the second turn and from 3–14 V/m in the third turn. The presence of the shallow positive slope of the DC profile at the modiolar end of the track results in a DC gradient (driving current away from the modiolus) that remains in the 0.5–2.0 V/m range over a 200–400-μm distance in scala vestibuli.

The DC gradients in scala vestibuli of the second and third turns are compared in Fig. 11. A mean DC gradient profile was calculated for each turn by first horizontally shifting the profiles along the depth axis by an amount that made the negative peaks line up at depth 0 μm (i.e., the same operation described for Fig. 8). The five shifted profiles from the second turn were averaged and plotted as squares and the three shifted profiles from the third turn were averaged and plotted as circles. Even though the magnitudes of the peaks differ by a factor of four in the second and third turn, the DC potential gradient deep in scala vestibuli of each turn is 1–2 V/m.

The shapes of the DC gradient profiles in scala vestibuli were compared by normalizing the profiles relative to the negative peak. The results of this normalization procedure are presented in Fig. 12 (*top*, second-turn data; *bottom*, third-turn data). The striking similarity of the

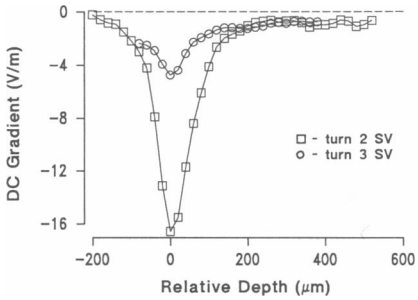

FIGURE 11 Average radial DC gradient profiles from scala vestibuli of the second and third turns. Before averaging, the DC gradient profiles of Fig. 10 were first shifted by an amount that made the negative peaks line up at depth 0 μm. The DC gradient profile collected along the first track in experiment GPC8 was not included in the average for the third turn.

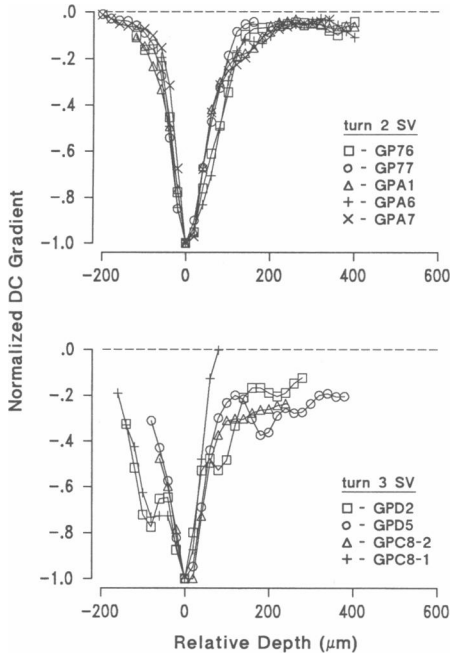

FIGURE 12 Normalized DC gradient profiles from scala vestibuli. Before normalizing the DC gradient profiles of Fig. 10, they were first shifted by an amount that made the negative peaks line up at depth 0 μm. The DC gradients were normalized by dividing the magnitude of the DC gradient at each point by the magnitude of the DC gradient at depth 0 μm. (*Top*) Second turn profiles. The division factors were as follows (in volts per meter): GP76 (14.8), GP77 (27.5), GPA1 (18.8), GPA6 (9.35), GPA7 (12.4). (*Bottom*) Third turn profiles. The division factors were as follows (in volts per meter): GPC8-1 (12.9), GPC8-2 (6.00), GPD2 (4.63), GPD5 (3.62).

normalized profiles implies that the shape of the DC gradient profile in scala vestibuli is independent of the magnitude of the DC potential gradient. A similar statement cannot be made of the scala-tympani DC gradients shown in Fig. 8. The modiolar slopes of the DC potential gradient profiles in scala tympani are similar to one another, regardless of the magnitude of the peak. No amount of shifting and scaling would make the scala-tympani DC potential gradients superimpose. In contrast, all of the DC potential gradient profiles in scala vestibuli of the second turn are, at least to a first approximation, translated and scaled versions of one another.

In contrast to the second-turn results, the magnitude of the DC gradient deep in scala vestibuli of the third turn is 20–40% of the negative peak. On the other hand, if one ignores the 100–200-μm depth range of experiments GPD2 and GPC8-1, then the shape of the negative peak is actually quite similar in the second and third turns. In experiment GPD2, the abrupt 100 μV shift in the DC potential in the 160–200-μm depth range raises suspicion about this part of the DC profile. The other third-turn profile, GPC8-1, was unusual in that an endocochlear potential (+65 mV) was encountered at depth 500 μm, indicating that the electrode penetrated through Reissner's membrane and into scala media. This may also explain why this track encountered the largest DC gradient in scala vestibuli of the third turn and may also explain the absence of a shallow slope of the DC profile at the modiolar end of the track.

Modulation of the standing current: the microphonic current

The importance of the cochlear standing currents for cochlear transduction derives from their modulation by acoustic stimulation. Radial tone-evoked potential gradients were calculated from field potentials collected along scala-tympani and scala-vestibuli tracks by computing the first spatial derivative (using computations similar to those used to calculate click-evoked radial potential gradients in scala tympani by Brownell et al., 1983). Acoustically-evoked potential gradients represent a modulation of the radial standing current. Standing currents in scala vestibuli (*top*) and scala tympani (*bottom*) and their modulation with a 200-Hz stimulus are shown in Fig. 13. The spatial profile of the modulation of the radial potential gradient is shown for two points in time corresponding to maximal displacement of the cochlear partition toward scala tympani (*triangles*) and toward scala vestibuli (*circles*) as inferred from the CM (von Békésy, 1951*b*).

Fig. 13 illustrates the reciprocal nature of the modulation of potential gradients in scala tympani and scala vestibuli. During scala-vestibuli displacement of the cochlear partition (*circles*), the modulation of the potential gradient is in the positive direction in scala vestibuli (i.e., toward the modiolus), whereas in scala tympani the modulation is in the negative direction (i.e., toward the

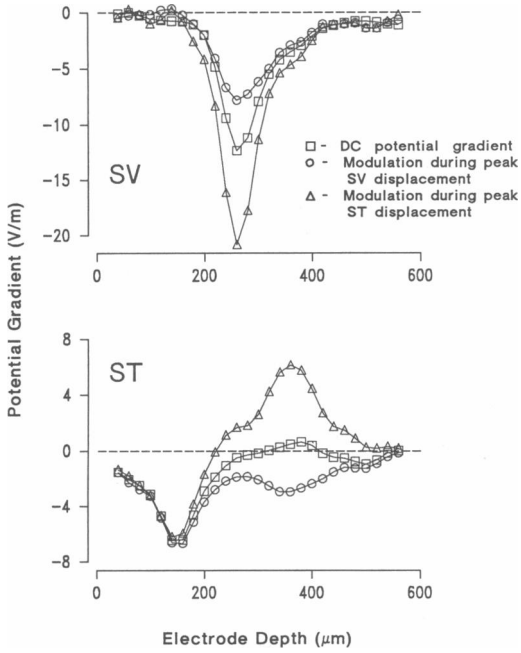

FIGURE 13 Standing currents in scala tympani (GPA9, *bottom*) and scala vestibuli (GPA7, *top*) and their modulation during 200 Hz acoustic stimulation. The DC potential gradients (*squares*) are the average of several profiles obtained along the same track (negative potential gradients indicate currents directed away from the modiolus). Two phases of the modulation of the DC potential gradient were selected for display. (*Circles*) Modulation during peak displacement of the cochlear partition towards scala vestibuli (as inferred from CM). During this phase of stimulation, the standing current normally flowing toward the spiral ligament is reduced in scala vestibuli (*top*) and augmented in scala tympani (*bottom*). The opposite direction of current modulation occurs during cochlear partition displacement towards scala tympani (*triangles*). Note that the modulation of the potential gradient is in register with the DC potential gradient in scala vestibuli, but is displaced ~200 μm towards the modiolus in scala tympani.

spiral ligament). During displacement of the cochlear partition toward scala tympani (*triangles*), the direction of potential gradient modulation is reversed relative to scala-vestibuli displacement: the potential gradient is modulated in the negative direction in scala vestibuli (i.e., toward the spiral ligament), whereas in scala tympani the modulation is in the positive direction (i.e., toward the modiolus).

A qualitative difference between radial potential gradient modulation in scala tympani and scala vestibuli is evident in the relation between the location of the standing current peak and the location of maximal modulation of the radial current. In the scala-vestibuli experiment shown, the peak of the radial standing current is at depth 240 μm (*squares*). During peak cochlear partition displacement toward scala vestibuli, the peak of the standing current through the scala-vestibuli pathway is reduced by a factor of two (*circles*). During peak cochlear partition displacement toward scala tympani, the peak of the radial standing current through the scala-vestibuli pathway is augmented by a factor of two (*triangles*). Thus, at least with acoustic stimuli of moderate intensity (80 dB SPL) the direction of radial current does not change in scala vestibuli.

In contrast, the peak of the radial standing current in scala tympani (depth, 160 μm) is not significantly modulated during acoustic stimulation. Peak modulation of the radial potential gradient is located ~200 μm modiolar to the standing current peak, a location where there is little or no radial component to the standing current. Thus, at this location in scala tympani (depth, 360 μm) the current actually changes direction during the different phases of the sinusoidal stimulus. During scala-vestibuli displacement radial current is directed toward the spiral ligament, whereas during scala-tympani displacement radial current is directed toward the modiolus.

DISCUSSION

Radial DC gradients in scala tympani and scala vestibuli

In a given preparation DC potential profiles and the computed DC gradients are reproducible over a period of several hours. This stability suggests that significant changes in the standing currents do not occur while the animal is alive, nor do the electrode penetrations alter the pattern of current flow. There is a rapid postmortem decrease in the radial DC gradient recorded from either scala tympani or scala vestibuli, implying that the standing current is dependent on oxidative metabolism (Zidanic et al., 1985; Brownell et al., 1986).

The most striking feature of radial DC gradient profiles in scala tympani and scala vestibuli of the second and third turns is the single large negative peak within or near the spiral ligament. This peak represents a standing current flowing away from the modiolus and into the spiral ligament. Modiolar to the large peak the DC gradient tapers off rapidly. The simplest interpretation of the shape of the DC gradient profiles is that the single large peak represents the potential gradient generated by a standing current as it flows through the spiral ligament. Several arguments can be presented to support the interpretation of large potential gradients in the spiral ligament.

The first is that the conductivity of the spiral ligament is likely to be lower than that of perilymph based on anatomical considerations. The spiral ligament is composed of loosely-packed cells in an extracellular matrix of fibers that provide an elastic support for the basilar membrane to the otic capsule. Whereas gross impedance

measurements have been made across the spiral ligament in vivo (Cannon, 1976), many assumptions must be made to calculate tissue conductivity. Measures of interstitial fluid conductivity have been obtained in other preparations that provide an insight to the question of spiral-ligament conductivity. In an in vitro isolated rat retina preparation, Hagins et al. (1970) determined that the extracellular conductivity in the interstitial space in the outer nuclear layer is five times less than extracellular fluid. Because the cell packing appears to be much less in the spiral ligament than in the outer nuclear layer of the retina, the conductivity ratio of perilymph to the spiral ligament is probably at most two to four. By Ohm's law (Methods, Eq. 6), the same current density will generate a larger potential gradient in a region of low conductivity (i.e., in the spiral ligament) than in a region of high conductivity (i.e., in the perilymphatic scalae).

A second reason for large potential gradients in the spiral ligament is based on electroanatomical considerations. The distance between the basilar membrane and the bone that separates adjacent cochlear coils is relatively large in the middle of scala tympani, but is smaller near the lateral wall (Figs. 2 and 14). The fluid space in scala vestibuli between the attachment of Reissner's membrane and the otic capsule is even smaller. If all of the current flowing through each chamber is recycled back to the stria vascularis via an extracellular route, then current density will be largest in the spiral ligament where the cross-sectional area orthogonal to the direction of the current is at a minimum.

Anecdotal evidence also supports the presence of large potential gradients in the spiral ligament. Micropipettes were observed through the dissecting microscope as they were advanced into scala vestibuli. Sometimes the electrode would bend as it made contact with the spiral ligament and then it would straighten after penetrating the spiral ligament. One consequence of electrode bending and slippage during data collection is that the tip of the pipette may remain at the same depth for several 20-μm advances of the microdrive spindle and then suddenly advance 40–100 μm on a subsequent depth increment. If radial potential gradients exist within the spiral ligament, then such irregularities in the travel of the electrode through the spiral ligament would give rise to abrupt changes in the measured DC potential and CM profiles. Discontinuities were found at lateral locations of the CM magnitude profiles along several forward data collection tracks (Zidanic, M., and W. E. Brownell, submitted for publication). These data support the interpretation that DC and CM potential gradient peaks are located within the spiral ligament bordering scala vestibuli.

Despite inter-animal variability in the radial DC gradients, the smallest DC gradients are recorded from scala tympani whereas the largest DC gradients are recorded from scala vestibuli. One explanation for large scala-vestibuli DC gradients is based on anatomical constraints for current flow from scala vestibuli into the spiral ligament. There is only a narrow portion of the spiral ligament, no more than 50 μm wide, that extends above the attachment of Reissner's membrane to the lateral wall. All of the current returning to the stria vascularis through scala vestibuli must "squeeze through" the spiral ligament at this location. On the other hand the spiral ligament is 100–150 μm wide at the level of the basilar membrane. Thus, even if similar current densities are present in the central portions of both scala tympani and scala vestibuli, a larger radial current density may be

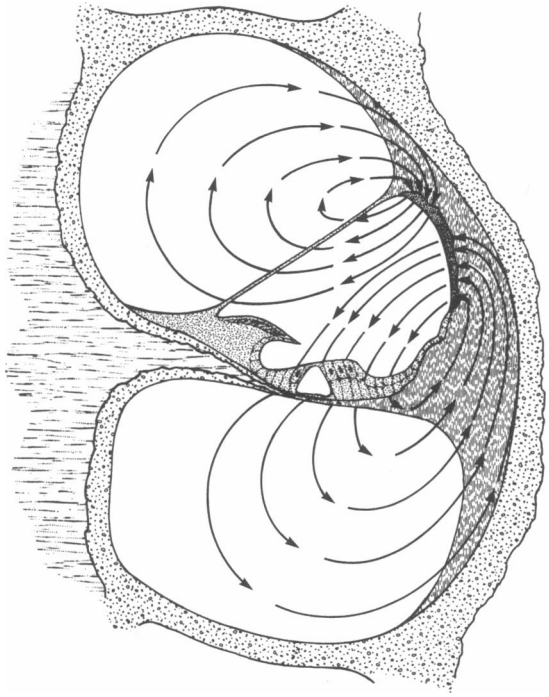

FIGURE 14 Model for standing currents in the cochlea in terms of current density field lines. The magnitude of current density at any particular location is determined by the local concentration of field lines. The direction of current is indicated with arrows along the field lines. The basic assumption of the model is that all current generated by the stria vascularis (*shaded area*) exits scala media and is recycled via scala tympani and scala vestibuli. Little or no current is presumed to flow through the bone that forms the boundary of each chamber with the modiolus, separates scala vestibuli and scala tympani of adjacent turns, and encapsulates the entire cochlea. This local flow of current results in a concentration of the current lines within the spiral ligament. A major pathway for current leakage from scala media is through the mechanically-sensitive transduction channels in the stereocilia of the hair cells. Current also is postulated to leak through Reissner's membrane and also through (or between) the supporting cells lateral to the organ of Corti. Figure from Brownell, 1990, and reprinted with permission of Williams & Wilkins.

present near the spiral ligament in scala vestibuli because the current must flow through a smaller cross-sectional area.

Variability of DC gradients across experiments

The magnitude of the large DC gradient peak near the lateral part of scala tympani tracks varied from 3 to 18 V/m. The shape of the DC gradient profiles in scala tympani varied as well. One significant source of variability is likely due to differences in the orientation of electrode tracks relative to the ideal track parallel to the basilar membrane. Electrode orientations of ±30° relative to the basilar membrane and distances of 0–200 μm from the basilar membrane could very well be possible across experiments. A technique has been developed to reconstruct electrode tracks from histological material (Cousillas et al., 1989). When this technique is combined with potential gradient measurements in scala tympani and scala vestibuli, an assessment of the effect of electrode orientation on the measured potential gradients will become possible.

For the experiments in scala vestibuli, the magnitude of the peak of the DC gradients differed by a factor of three, although the shape of the DC gradient profiles remained constant. As in scala tympani, the differences in magnitude could result from variability in electrode track orientation relative to the ideal track parallel to Reissner's membrane. Alternatively, the tissue conductivity along the electrode track or the amount of leakage current through Reissner's membrane could vary across experiments. While it is rather unlikely that the conductivity of perilymph is significantly different across experiments, surgical trauma to the spiral ligament could lead to a change in conductivity. Such a change in conductivity would be expected to alter the local current density field near the spiral ligament, with a minimal effect on the field in the middle of the scala vestibuli chamber. If the standing current through Reissner's membrane is the same across experiments, and differences in the conductivity of the spiral ligament are responsible for the observed differences in magnitude of the DC gradient peaks, then the DC gradient in the middle of scala vestibuli should not vary significantly across experiments. However, the fact that the magnitude of the DC gradient near the modiolus in scala vestibuli remains a fixed percentage of the magnitude of the DC gradient peak near the lateral wall (~5%) argues that differences in tissue conductivity of the spiral ligament are not likely to be responsible for the DC gradient magnitude differences. The variability more likely results from differences in the amount of current leaking through Reissner's membrane or through that part of the spiral limbus facing scala vestibuli.

A second possible source of variability of the DC gradient profiles is trauma associated with otic capsule surgery. The threshold shifts of the CAP of 5–10 dB at CF that were usually measured following otic capsule surgery support this view. In contrast to manipulations such as noise damage or aminoglycoside administration that have relatively specific effects on hair cells, the otic capsule surgery used to gain access to scala tympani or scala vestibuli may damage accessory structures as well, including the stria vascularis and Reissner's membrane. Traumatic events leading to a change in cochlear currents may be quite subtle and not easily identified with the light microscopic histological processing used in this study. For example, hair cell stereocilia damage could increase the EP (Konishi et al., 1979) and drive more current through leakage pathways, including scala vestibuli. Reduced blood flow to the stria vascularis could reduce current through all pathways out of scala media. Surgical trauma to Reissner's membrane that disrupts the tight junctions could increase its conductivity leading to an increased leakage current through the scala-vestibuli pathway, a concomitant reduction of the EP, and a reduced current through the hair cells and the scala-tympani pathway.

A consistent finding in the histological material was the detachment of the spiral ligament from the otic capsule in the region of the exposure. Complete detachment of the spiral ligament from the floor of scala tympani or from the roof of scala vestibuli could permit current to short circuit around the presumably less conductive spiral ligament. In addition, the histology of several scala-vestibuli and scala-media experiments showed detachment of the spiral ligament from the lateral wall resulting in Reissner's membrane sagging onto the tectorial membrane in the region of the exposure. If such an event is not an artifact of the histological processing of the tissue but actually occurs while the experiment is in progress, then a change in the static position of the stereocilia could be induced. This could lead to either an increase or decrease in the resting current through the hair cell transduction channels depending on the direction of stereocilia deflection (Hudspeth and Corey, 1977). The concomitant change in the EP would indirectly lead to a change in current through the scala-vestibuli pathway.

Relation of microphonic current to standing current

The peak of the microphonic current in scala tympani is located ~200 μm modiolar to the standing current peak (Fig. 13). Thus, if the assignment of the DC gradient peak to the spiral ligament is correct, then the peak of the

radial microphonic current is located within scala tympani just below or lateral to the outer hair cells. The presence of microphonic currents in scala vestibuli argues that at least some of the current that is modulated by the hair cells is shunted through the scala-vestibuli pathway. A likely pathway for current between the hair cells and scala vestibuli is through scala tympani and the spiral ligament. However, because of the spatial separation of the radial DC and CM current peaks in scala tympani, very little radial current is modulated in the region of the DC gradient peak, i.e., the presumed location of the spiral ligament. This result implies that (*a*) either the net current through the scala-tympani pathway does not change during acoustic stimulation or (*b*) that both the magnitude and direction of the current through the spiral ligament bordering scala tympani change such that the radial component of the current remains unchanged. If the first possibility is correct, then alternative pathways must be considered for current flow from scala tympani to the lateral wall of scala vestibuli.

The Hensen's cells of the organ of Corti are electrically coupled by gap functions (Iurato et al., 1976; Gulley and Reese, 1976; Santos-Sacchi, 1984). These cells may be part of an electrical network that provides a low-impedance transcellular pathway for current flow from the spaces of Nuel (the large extracellular spaces around the outer hair cells) to a region of the spiral ligament near the stria vascularis. Such an intracellular pathway could be shielded from the extracellular currents measured in this study and could provide part of the pathway for the modulation of current that is shunted from the hair cells to scala vestibuli.

If the microphonic currents in scala tympani do not make their way to scala vestibuli, then where do they go? One possibility is that an alternative leakage pathway of the endolymph/perilymph barrier is present lateral to the organ of Corti and modiolar to the spiral ligament, placing it in the external sulcus. During acoustic stimulation, there could be a reciprocal modulation of current through the hair cells and this leakage pathway, i.e., when current is increased through the hair cells, current through the leakage pathway is reduced and vice versa. Such a local pathway of reciprocal currents could maintain the net current through scala tympani relatively constant during acoustic stimulation.

Other evidence can also be brought forth in support of a leakage current through the external sulcus. Such a leakage current could explain the presence of 5–10 mV positive DC shifts that were stable over a 20–50-μm range along tracks in several scala-tympani experiments. On subsequent excursions along the same track, the small positive DC shifts were replaced with the EP (probably because the micropipette traversed a slightly different path through the spiral ligament) that was recorded only over a 40–60-μm range. The CM phase changed very little upon entry into scala media and then shifted ~180° when the DC returned to the near-zero level after exiting scala media. Such a short track through scala media with these DC and CM characteristics could only result from the electrode passing into scala media in the region of the spiral prominence (the area bordering scala media below the stria vascularis), passing through the external sulcus in scala media, and exiting into scala tympani. Thus, the electrode excursions with the 5–10-mV positive shifts preceding the excursions that penetrated scala media most likely passed just below the external sulcus.

Standing currents through hair cells

Because the standing currents are modulated by acoustic stimuli, at least part of the standing current can be assumed to flow out of scala media through the mechanically-sensitive transduction channels in the sterocilia of the inner and outer hair cells. The microphonic currents reduce and enhance the standing current during opposite phases of the stimulus cycle, consistent with a resting current flowing through the transduction channels in silence.

A significant radial DC gradient (1–2 V/m) representing a standing current away from the modiolus is present in scala vestibuli over the 600-μm length of the track. One explanation of this result is that most of the current that flows through the scala-vestibuli pathway leaks through scala media near the modiolus, where Reissner's membrane attaches to the spiral limbus. In contrast, there is an absence of a radial DC gradient at the modiolar portion of the track in scala tympani. The DC profiles in scala tympani generally reach a plateau value within 400 μm of the starting point of the track. The absence of a radial potential gradient at the modiolar portion of the scala-tympani tracks indicates either (*a*) that there is no current density at this location, or (*b*) that the current has changed direction from a radial orientation near the spiral ligament to a vertical orientation. The latter possibility is more likely because the modiolar portion of the track is probably located below the organ of Corti. The current that flows through the outer hair cells would be expected to be oriented in the vertical direction near the hair cells as it spreads out into scala tympani. The current through the single row of inner hair cells (located about 100 μm modiolar to the three rows of outer hair cells) is probably not large enough to influence the current density field below the outer hair cells. An alternative possibility is that some of the current through the inner hair cells may leak into the modiolus and return to the stria vascularis via a spiral-limbus/scala-vestibuli pathway or through the vasculature.

A current density model for standing currents

These results demonstrate that radial standing currents are present in both scala tympani and scala vestibuli of the guinea-pig cochlea. In each of these two cochlear chambers, current is directed into the spiral ligament. Because the standing current flows in the same direction in both scala tympani and scala vestibuli, one possibility to consider is that the current from one cochlear chamber leaks into the adjacent chamber of the next turn through the thin bone that separates the cochlear turns. If this is a significant pathway for DC currents, then trans-coil current should also be present during very low-frequency stimulation. However, at 50 Hz, where there is little or no phase lag of the CM from base to apex (Dallos and Cheatham, 1971; Oshima and Strelioff, 1983; Zidanic, M., unpublished observations), not only are low-frequency microphonics out of phase in scala tympani versus vestibuli (Dallos et al., 1971) but the modulation of radial current is in the opposite direction in scala tympani versus scala vestibuli.

Because trans-coil currents appear unlikely, models for intracochlear currents can be restricted in local flow in the transverse plane and longitudinal flow along the coiling scalae. A model of current flow in terms of current density field lines is depicted in Fig. 14. According to this model, current is recycled within the same transverse cochlear cross-section. The energy source for the current lies within the stria vascularis, entering scala media through the apical membrane of the marginal cells that form the lateral wall of scala media. The current exits scala media through the organ of Corti and Reissner's membrane and returns via scala tympani and scala vestibuli to be recycled back to the stria. The results of this study support this model because standing currents are not seen directed into the modiolus in either scala tympani or scala vestibuli. This model is also consistent with experiments that have shown that potassium ions are actively taken up from scala tympani to scala media (Konishi et al., 1978) and that the primary source of endolymph is not from the vascular system (Wada et al., 1979).

The silent current and cochlear energetics

An estimate of the total current generated by a given transverse wedge of the cochlea can be derived from the measurements presented in this study. While potential gradients as large as 10–15 V/m are recorded along radial tracks, the large peak is within the first 200 μm of the track and could be due to a low conductivity of the spiral ligament. On the modiolar side of the DC gradient peak, the radial potential gradient is in the 1–2 V/m range in both scala tympani and scala vestibuli. Based on a conductivity of 2 S/m for perilymph (von Békésy, 1951*a*), this gradient corresponds to a current density of 2–4 A/m^2. If the radial flow of current is uniform throughout the 200-μm depth of each perilymphatic scala, then a total current of 0.8–1.6 μA circulates through the endolymph/perilymph barrier in a 1-mm wedge of the cochlea.

Calculations on the metabolic consequences of the silent current can be made from the above estimate of the total circulating current (Table 1). If half of the current crossing the endolymph/perilymph barrier is carried by K^+, then the half-time of K^+ exchange in endolymph is 36 min. A similar calculation for chloride using a transport number of 0.25 results in a 59-min half-time of exchange. These values compare well with the values of 55 and 69 min for K^+ and Cl^-, respectively, that have been measured using radioactive tracer techniques (Konishi and Hamrick, 1978; Konishi et al., 1978). The calculated value for ATP consumption required to support the K^+

TABLE 1 Metabolic consequences of the silent current

Based on a resting current of 1 μA in a 1-mm section of the cochlea	
A. Energetics of 1-mm section of stria vascularis	
Equivalent K^+ flux per mm*	3.11 10^{-10} mole min^{-1}
Total K^+ in 1-mm segment‡	1.6 10^{-8} moles
K^+ transport rate constant	0.0194 min^{-1}
Half-time K^+ exchange§	35.7 min
ATP consumption per mm‖	2.59 10^{-12} mole s^{-1}
B. ATP utilization of second turn stria (Kuijpers and Bonting, 1969)	
Protein content of stria per mm¶	3 μg
$(Na^+ + K^+)$-ATPase activity (second turn)	7.03 moles kg^{-1} h^{-1}
ATP consumption per mm (second turn)	5.86 10^{-12} moles s^{-1}
C. Marginal cell energetics	
Current through luminal membrane of average marginal cell (4,250 per mm)**	235 pA
Number of $(Na^+ + K^+)$-ATPases per marginal cell‡‡	3.67 10^6
Density of $(Na^+ + K^+)$-ATPase in basolateral cell membrane (500 μm^2)	7,339 μm^{-2}

*50% of current carried by K^+.
‡$[K^+]$ = 160 mM, endolymph volume of 1-mm section: 0.1 μl.
§Based on two compartment model of Konishi et al. (1978).
‖2 K^+ transported per ATP hydrolyzed.
¶12-μg dry wt of 4-mm section (Kuijpers and Bonting, 1969).
**Calculated based on anatomical data of Forge et al., 1987.
‡‡50% of total current carried by $(Na^+ + K^+)$-ATPase, turnover rate 100 per second.

transport agrees within a factor of 2.5 from the value derived from enzyme activity measurements of Kuijpers and Bonting (1969). Thus the magnitude of the silent current we have measured is within the range expected from kinetic experiments and has energy requirements within the capabilities of the $(Na^+ + K^+)$-ATPase system of the stria vascularis.

The silent current enters scala media through ~4,250 marginal cells per millimeter length of the cochlea (using anatomical data of Forge et al., 1987), corresponding to an average current of 188–376 pA/marginal cell. By comparison, Hagins et al. (1970) calculated an average current of 70 pA per retinal rod to support the dark current. The standing current through the hair cells of the organ of Corti may be as large as the 500 pA/hair cell (Brownell et al., 1983) cochlear microphonic current.

The high K^+ content of endolymph combined with the positive endolymphatic potential generates a large potential gradient for K^+ across the apical hair cell membrane. Permeability of the hair cell transduction channel to K^+ (Corey and Hudspeth, 1979) will lead to a steady K^+ influx, alleviating the need for sodium-potassium pumps in the basolateral hair cell membrane. The demand for a direct blood supply to the organ of Corti is reduced because cochlear hair cells can carry out mechanoelectrical transduction without expending a great deal of energy. The absence of a nearby capillary bed reduces the mechanical noise of blood flow and ateriole pulsations to a minimum.

The mammalian cochlea appears to have evolved an elegant mechanism incorporating an active mechanical detector on the verge of instability (Gold, 1948) that allows it to detect motion near the thermal noise floor. In a manner that has yet to be fully revealed, the electromechanical feedback capability of the outer hair cells (Brownell et al., 1985), powered by the silent current and dynamically modulated by acoustic stimuli, is poised within the micromechanical structure of the organ of Corti to endow the mammalian cochlea with a very fine sensitivity and frequency selectivity.

We are grateful to Drs. H. Cousillas, P. Manis, M. Sachs, G. Spirou, and E. Young of the Center for Hearing Sciences at The Johns Hopkins University and to Drs. W. Luttge, J. Zengel, and J. Middlebrooks of the Department of Neuroscience at the University of Florida for providing helpful comments on this manuscript. We thank A. Salt for his suggestions concerning the ion transport rate calculations. G. Spirou and P. Dulguerov participated in the early phases of these experiments. M. A. Smith and C. Strathmeyer provided the histological processing of the cochleas and the surgical preparation of the animals. Fig. 2 was prepared by the Graphic Arts department at the University of Florida and Fig. 14 was prepared by the Graphic Arts department at The Johns Hopkins University.

This work supported by NIH grant NS23567 from NIDCD to WEB and a Deafness Research Foundation grant to P. Dulguerov.

REFERENCES

Brownell, W. E. 1990. Outer hair cell electromotility and otoacoustic emissions. *Ear and Hearing.* 11:82–92.

Brownell, W. E., P. B. Manis, M. Zidanic, and G. A. Spirou. 1983. Acoustically evoked radial current densities in scala tympani. *J. Acoust. Soc. Am.* 74:792–800.

Brownell, W. E., C. R. Bader, D. Bertrand, and Y. de Ribaupierre. 1985. Evoked mechanical responses in isolated cochlear outer hair cells. *Science (Wash. DC).* 227:194–196.

Brownell, W. E., M. Zidanic, and G. A. Spirou. 1986. Standing currents and their modulation in the cochlea. *In* Neurobiology of Hearing: The Cochlea. R. A. Altschuler, D. W. Hoffman, and R. P. Bobbin, editors. Raven Press, New York. 91–107.

Cannon, M. W. 1976. Electrical impedances, current pathways, and voltage sources in the guinea pig cochlea. Ph.D. dissertation. Syracuse University, Syracuse, NY.

Corey, D. P., and A. J. Hudspeth. 1979. Ionic basis of receptor potential in a vertebrate hair cell. *Nature (Lond.)* 281:675–677.

Cousillas, H., M. Zidanic, and W. E. Brownell. 1989. Longitudinal DC and CM potential gradients in scala media of the guinea pig cochlea. *Abstr. Midwinter Res. Meeting Assoc. Res. Otolaryngol.* 12:130.

Dallos, P., and M. A. Cheatham. 1971. Travel time in the cochlea and its determination from cochlear-microphonic data. *J. Acoust. Soc. Am.* 49:1140–1143.

Dallos, P., Z. G. Schoeny, and M. A. Cheatham. 1971. On the limitations of cochlear-microphonic measurements. *J. Acoust. Soc. Am.* 49:1144–1154.

Davis, H. 1953. Energy into nerve impulses: the inner ear. *Adv. Sci.* 9:420–425.

Duvall, A. J., and C. R. Sutherland. 1972. Cochlear transport of horseradish peroxidase. *Ann. Otol. Rhinol. & Laryngol.* 81:705–714.

Fex, J. 1959. Augmentation of cochlear microphonics by stimulation of efferent fibers to the cochlea. *Acta Oto-laryngol.* 50:540–541.

Fex, J. 1967. Efferent inhibition in the cochlea related to hair cell dc activity: study of postsynaptic activity of the crossed olivocochlear fibers in the cat. *J. Acoust. Soc. Am.* 41:666–675.

Forge, A., A. Wright, and S. J. Davies. 1987. Analysis of structural changes in the stria vascularis following chronic gentamicin treatment. *Hearing Res.* 31:253–266.

Freeman, J. A., and C. Nicholson. 1975. Experimental optimization of current source-density technique for anuran cerebellum. *J. Neurophysiol.* 38:369–382.

Geisler, C. D. 1974. Model of crossed olivocochlear bundle effects. *J. Acoust. Soc. Am.* 56:1910–1912.

Gold, T. 1948. Hearing. II. The physical basis of the action of the cochlea. *Proc. R. Soc. Lond B Biol Sci.* 135:492–498.

Gulley, R. L., and T. S. Reese. 1976. Intercellular junctions in the reticular lamina of the organ of Corti. *J. Neurocytol.* 5:479–507.

Hagins, W. A., R. D. Penn, and S. Yoshikami. 1970. Dark current and photocurrent in retinal rods. *Biophys. J.* 10:380–412.

Hudspeth, A. J., and D. P. Corey. 1977. Sensitivity, polarity, and conductance change in the response of vertebrate hair cells to controlled mechanical stimuli. *Proc. Natl. Acad. Sci. USA.* 74:2407–2411.

Iurato, S., K. Franke, L. Luciano, G. Wermbter, E. Pannese, and E. Reale. 1976. Fracture faces of the junctional complexes in the reticular membrane of the organ of Corti. *Acta Oto-laryngol.* 81:36–47.

Jahnke, K. 1975. The fine structure of freeze-fractured intercellular junctions in the guinea pig inner ear. *Acta Oto-laryngol. Suppl.* 336:1–40.

Johnstone, J. R., V. A. Alder, B. M. Johnstone, D. Robertson, and G. K. Yates. 1979. Cochlear action potential threshold and single unit thresholds. *J. Acoust. Soc. Am.* 65:254–257.

Konishi, T., and P. E. Hamrick. 1978. Ion transport in the cochlea of the guinea pig. II. Chloride transport. *Acta Oto-laryngol.* 86:176–184.

Konishi, T., P. E. Hamrick, and P. J. Walsh. 1978. Ion transport in guinea pig cochlea. I. Potassium and sodium transport. *Acta Oto-laryngol.* 86:22–34.

Konishi, T., A. N. Salt, and P. E. Hamrick. 1979. Effects of exposure to noise on ion movement in guinea pig cochlea. *Hearing Res.* 1:325–342.

Kuijpers, W., and S. Bonting. 1969. Studies on the (Na^+-K^+)-activated ATPase. XXIV. Localization and properties of ATPase in the inner ear of the guinea pig. *Biochim. Biophys. Acta.* 173:477–485.

Liberman, M. C., and L. W. Dodds. 1984. Single-neuron labeling and chronic cochlear pathology. II. Stereocilia damage and alterations of spontaneous discharge rates. *Hearing. Res.* 16:43–53.

Oshima, W., and D. Strelioff. 1983. Responses of gerbil and guinea pig auditory nerve fibers to low-frequency sinusoids. *Hearing Res.* 12:167–184.

Penn, R. D., and W. A. Hagins. 1969. Signal transmission along retinal rods and the origin of the electroretinographic a-wave. *Nature (Lond).* 223:201–205.

Robertson, D., A. R. Cody, G. Bredberg, and B. M. Johnstone. 1980. Response properties of spiral ganglion neurons in cochleas damaged by direct mechanical trauma. *J. Acoust. Soc. Am.* 67:1295–1303.

Salt, A. N., and T. Konishi. 1986. The cochlear fluids. *In* Neurobiology of Hearing: The Cochlea. R. A. Altschuler, D. W. Hoffman, and R. P. Bobbin, editors. Raven Press, New York. 108–122.

Santos-Sacchi, J. 1984. A reevaluation of cell coupling in the organ of Corti. *Hearing Res.* 14:203–204.

Sewell, W. F. 1984. The relation between the endocochlear potential and spontaneous activity in auditory nerve fibres of the cat. *J. Physiol. (Lond.).* 347:685–696.

Siegel, J. H., and W. E. Brownell. 1986. Synaptic and Golgi membranes recycling in cochlear hair cells. *J. Neurocytol.* 15:311–328.

Smith, C. A., O. H. Lowry, and M. L. Wu. 1954. The electrolytes of the labryrinthine fluids. *Laryngoscope.* 64:141–153.

Tasaki, I., and C. S. Spyropoulos. 1959. Stria vascularis as source of endocochlear potential. *J. Neurophysiol.* 22:149–155.

Tasaki, I., H. Davis, and D. H. Eldredge. 1954. Exploration of cochlear potentials in guinea pig with a microelectrode. *J. Acoust. Soc. Am.* 26:765–773.

Teas, D. C., T. Konishi, and D. W. Nielson. 1970. Electrophysiological studies on the spatial distribution of the crossed olivocochlear bundle along the guniea pig cochlea. *J. Acoust. Soc. Am.* 51:1256–1264.

von Békésy, G. 1951*a*. The coarse pattern of the electrical resistance in the cochlea of the guinea pig (electroanatomy of the cochlea). *J. Acoust. Soc. Am.* 23:18–28.

von Békésy, G. 1951*b*. Microphonics produced by touching the cochlear partition with a vibrating electrode. *J. Acoust. Soc. Am.* 23:29–35.

von Békésy, G. 1952. DC resting potentials inside the cochlear partition. *J. Acoust. Soc. Am.* 24:72–76.

Wada, J., J. Kambayashi, D. C. Marcus, and R. Thalmann. 1979. Vascular perfusion of the cochlea: effect of potassium-free and rubidium-substituted media. *Arch. Otorhinolaryngol. Beg.* 225:79–81.

Zidanic, M., W. E. Brownell, G. A. Spirou, and P. B. Manis. 1984. Standing currents in scala tympani of the guinea pig cochlea. *Abstr. Midwinter Res. Meeting Assoc. Res. Otolaryngol.* 7:82.

Zidanic, M., W. E. Brownell, and G. A. Spirou. 1985. Modulation of radial standing currents. *Abstr. Midwinter Res. Meeting Assoc. Res. Otolaryngol.* 8:84.

Zidanic, M., W. E. Brownell, and P. Dulguerov. 1987. DC and CM gradients in the guinea pig cochlea. *Abstr. Annu. Meeting Soc. Neurosci.* 17:539.